Electronic structure, phase stability, and cohesive properties of Ti_2XAl (X=Nb, V, Zr)

C. Ravi, P. Vajeeston, S. Mathijaya, and R. Asokamani
Department of Physics, Anna University, Chennai-25, India
(Received 19 May 1999)

The self-consistent tight-binding linear muffin-tin orbital method was employed to calculate the electronic structure and the total energy of Ti_2XAl (X=Nb, V, Zr) in $B2$, $D0_{19}$, and O (orthorhombic) phases and the results were used to study the phase stability and cohesive properties of these intermetallic compounds. Our theoretical calculation shows that the $B2$ phase is the most stable phase of Ti_2NbAl as observed by experimentalists. However, the three phases are close in energy indicating the possibility of the presence of all these phases in equilibrium over a range of temperatures, which is in accordance with experimental observations. Our calculations predict that Ti_2VAl is more stable in the $B2$ phase whereas Ti_2ZrAl is more stable in the $D0_{19}$ phase. We also report the calculated equilibrium lattice parameters, cohesive energies, heats of formation, and bulk modulii of these systems, and a possible comparison of the calculated quantities with the available experimental data is made. From our studies we are made to conclude that the concept of pseudogaps which has been very much emphasized for binary intermetallics does not carry so much significance with respect to ternary systems. [S0163-1829(99)05047-X]

I. INTRODUCTION

Intermetallic alloys based on Ti_3Al ($\alpha 2$ phase) have been studied extensively over the past two decades as potential high-temperature structural materials. The interest in Ti_3Al is further encouraged by the recent demand for the Ti-Al based alloys because of their superior specific strength and oxidation resistance. Limited ductility and toughness at low temperature are serious disadvantages in intermetallics. One of the processes to improve ductility and toughness is the crystal-structure conversion from a complex structure to a more simple close-packed structure by the addition of substitutional elements, as demanded by von Mises criterion for uniform deformation.[1]

The development of engineering alloys based on Ti_3Al is centered on the addition of Nb at levels up to about 25% to replace titanium in compositions based on Ti-(21–25) Al. Three phases are found to be important in the determination of phase equilibrium in these alloys. The first one is the $\alpha 2$ phase based on the stoichiometric Ti_3Al which has a $D0_{19}$ ($hP8$) structure with $P6_3/mmc$ symmetry. This structure is characterized by an atomic arrangement on the closed-packed (0001) planes which ensures that Al atoms share bonds only with Ti atoms in the nearest-neighbor positions, and which can be described in terms of four interpenetrating sublattices of which three contain Ti atoms and one contains Al atoms. It has been shown that Nb and other alloying additions such as Zr, Hf, and Mo all substitute the Ti sites in this crystal structure[2,3] [Fig. 1(a)]. The existence of an ordered $B2$ ($cP2$) phase is well known to be centered around the Ti_2NbAl composition. It has been shown that Ti and Al atoms occupy the two separate primitive sublattices constituting the structure while Nb occupies, in the main, the Al sublattice[4] [Fig. 1(b)]. Alloying additions such as Mo and V substitute in the Al sublattice while Zr and Hf substitute in the Ti sublattice.[3] The third important phase is the O (orthorhombic) phase, identified first by Banerjee *et al.*,[5] which is shown to possess a $Cmcm(oC16)$ symmetry with an orthorhombic structure that can be viewed as a slightly distorted form of the $\alpha 2$ phase [Fig. 1(c)]. The O phase has so far been identified[6] in only one other ternary Ti-Al-X system and it is Ti-Al-V. The O phase behaves very similar to the $\alpha 2$ phase in terms of the transformation characteristics. Important exceptions are the massive decomposition of the $B2$ phase in the temperature range 500 °C–900 °C to O or $\alpha 2$ which results in dramatically different phase distributions. In the Nb-enriched Ti_2NbAl composition, the sequence of transformation is complicated, as the alloy passes through the $\alpha 2 + B2$, $\alpha 2 + B2 + O$, and $O + B2$ phase fields on cooling. Kumfert and Leyens[7] report, after aging at 960 °C for 0.5 h, a three-phase mixture $[\alpha 2 + \beta_0 + O]$. The work of Blackburn and Smith[8] clearly demonstrates that plasticity at room temperature could be obtained by the addition of enough Nb (>10%) to stabilize the high-temperature phase of titanium in the $\alpha 2$ structure.

Ti_3Al deforms primarily by an a slip on the prismatic planes with the Nb addition increasing the propensity for a basal a slip. Twinning is excluded by the ordered structure. Thus only four independent slip systems exist in polycrystal-

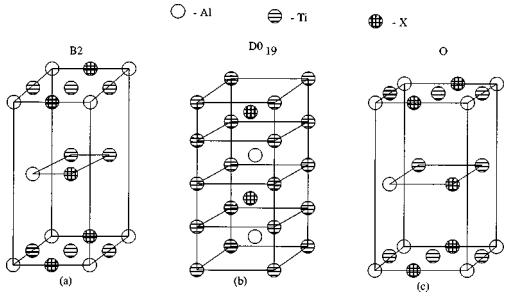

FIG. 1. Crystal structures in a Ti_2XAl system; (a) $D0_{19}$ structure where $a=b\neq c$ and $\alpha=\beta=90°$, $\gamma=120°$, (b) $B2$ supercell, and (c) orthorhombic (O) structure where $a\neq b\neq c$ and $\alpha=\beta=\gamma=90°$.

line material. The Nb addition increases the tendency for a basal slip and perhaps a homogeneous prismatic slip but does not increase the propensity for a *c* component slip. In contrast to the $\alpha 2$ behavior, a profuse *c* component slip of both [102] and $\langle 114 \rangle$ is observed in the *O* phase. The *B*2 distributions that avoid $\alpha 2/\alpha 2$ grain boundary contact are more effective in imparting ductility. The ability of the *B*2 phase at low volume fractions to impart ductility is directly related to its effect in increasing strain values at which the local critical stress for cleavage of $\alpha 2$ is realized. At higher volume fractions, the *B*2 phase acts as a barrier to crack extension from $\alpha 2$, and therefore the ductility rises steeply. Nevertheless, the single phase *B*2 is itself brittle at large grain size because of slip inhomogenity and it fractures by shear decohesion in intense slip bands. Since the *B*2 phase also has a higher yield strength, it plays the dual role of ductilizing and strengthening the $\alpha 2$ phase.[9] The class of orthorhombic titanium aluminide alloys currently appears to offer the best matrix material in titanium matrix composites (TMC's) designed for elevated temperature aircraft engine applications.[10]

Quantum-mechanical calculations from first principles, which are based on the local-density functional (LDF) approximations, can now predict the relative energies of different simple structure types. For example, from the heats of formation of the titanium aluminides, calculated by van Schilfgaarde *et al.*,[11] the LDF approximation predicts correctly the hexagonal $D0_{19}$ structure of Ti_3Al and the tetragonal $D0_{22}$ structure of $TiAl_3$. More importantly, it is capable of predicting the proximity in energy of competing metastable phases.[12]

We believe that so far there is no theoretical study on Ti_2XAl (X=Nb, V, Zr) compounds in the *B*2, $D0_{19}$, and *O* phases and the number of experimental studies are also limited. Reliable information, such as cohesive energy, heat of formation, and bulk modulii are also lacking. It is realized that strength, toughness, and ductility increase with Nb substitution. There is very little understanding on the mechanisms that lead to the ductility improvement by ternary and quaternary additions. The first-principle total-energy calculations on the three phases of these intermetallic compounds will improve the understanding of the relative phase stability among the competing phases, cohesive properties, and bonding properties. Rigorously, density-functional theory yields total energy and charge density only in the ground state ($T=0$ K). Also, lattice vibrations are not taken into account in our study. Therefore, our calculations are valid for high temperatures only as long as the entropy effects are sufficiently small. In principle, configurational entropies could be calculated on the basis of density-functional total energies[13] but such a computationally demanding task has not been initiated so far. It is worth recalling that the effective cluster interactions obtained from the total-energy band-structure studies have been used in conjunction with the cluster-variation method to construct the composition-temperature phase diagram of binary alloys.[14] So, the total-energy study of these systems in different structures becomes considerably important to construct the phase diagram theoretically. In the present study we discuss the electronic structure, chemical bonding, and the relative stability of Ti_2XAl (X=Nb, V, Zr) in *B*2, $D0_{19}$, and orthorhombic structures. This paper is presented in five sections. In Sec. II details with regard to the practical aspects of the linear muffin-tin orbital method along with the crystal-structural aspects are discussed. In Sec. III the structural properties and phase stability are disscussed in terms of total energy, heat of formation, and cohesive energy. Section IV deals with the electronic band structure and density of states (DOS) obtained from our calculations. The summary and conclusions are presented in Sec. V.

II. CRYSTAL STRUCTURE AND COMPUTATIONAL DETAILS

The crystal structures of Ti_2XAl in the *B*2, $D0_{19}$, and *O* phases are shown in Fig. 1. In the case of the *B*2 structure, an eight-atom supercell was constructed in which the cubic cell was extended four times in the *z* direction. The resulting cell has a simple tetragonal structure with a basis of eight atoms. The $D0_{19}$ phase is a hexagonal lattice with a basis of eight atoms and the *O* phase is an orthorhombic lattice with the same eight-atom basis. We have used the first-principles self-consistent tight-binding linear muffin-tin orbital (TB-LMTO) method within the local-density approximation with the use of the exchange-correlation potential of von Barth–Hedin to calculate the electronic structure and total energy of Ti_2XAl systems. Combined correction terms are also included, which account for the nonspherical shape of the atomic cells and the truncation of higher partial waves inside the sphere so as to minimize the errors in the LMTO method. The details of the method are well described in the literature.[15–18] In all our calculations reported here, the Wigner-Seitz (WS) sphere radii that were used lead to an overlap of about 8%. The average Wigner-Seitz radius was scaled so that the total volume of all the spheres is equal to the equilibrium volume of the unit cell. We have included *s*, *p*, *d*, and *f* partial waves in the calculations, and treat the core electrons fully relativistically and the valence electrons semirelativistically (i.e., neglecting spin-orbit coupling). The tetrahedran method of the Brillouin-zone (i.e., *k* space) integrations has been used with its latest version, which avoids misweighing and corrects errors due to the linear approximation of the bands inside each tetrahedron. The self-consistent iterations were continued until an an accuracy of 10^{-5} Ry was achieved in the eigenvalues. The eigenvalues were calculated at 512, 768, and 768 *k* points in the irreducible wedge of the tetragonal (*B*2), hexagonal ($D0_{19}$), and orthorhombic (*O*) Brillouin zones (BZ), respectively. The calculations were done at different cell volumes for each phase and the corresponding total energies were evaluated.

III. EQUILIBRIUM AND COHESIVE PROPERTIES

The cohesive energy is a measure of the strength of the forces which bind atoms together in the solid state. In order to understand the intergranular fracture mechanism of structural intermetallics, the estimation of the energy absorbed by bond stretching and breaking off along grain boundaries is necessary. In this connection, the cohesive energies of Ti_2XAl (X=Nb, V, Zr) in *B*2, $D0_{19}$, and orthorhombic

TABLE I. Structural and cohesive properties of the three phases of Ti_2NbAl.

	$B2$		$D0_{19}$		$O\,(A_2BC)$	
Ti_2NbAl	Calc.	Expt.[a]	Calc.	Expt.[a]	Calc.	Expt.[a]
Lattice parameters (a.u.)	$a=6.050$	6.198	$a=10.774$	10.960	$a=11.337$	11.414
			$c=8.731$	8.881	$b=18.057$	18.179
					$c=8.767$	8.825
			$c/a=0.818$	0.810	$a/b=0.627$	0.640
					$c/b=0.485$	0.489
Cohesive energy E_{coh} (eV/atom)	11.339		11.307		11.135	
Heat of formation ΔH (eV/atom)	-0.239		-0.208		-0.036	
$N\,(E_F)$(states/Ry/cell)	95		102		105	
Fermi energy E_F (Ry)	-0.063		-0.038		-0.047	
Bulk modulus B (Mbar)	1.454		1.524		1.359	1.23[b]
B'	6.106		6.224		6.276	

[a]Reference 7.
[b]Reference 23.

phases are calculated. For the study of the phase equilibrium, the cohesive energy is more descriptive than the total energy, since the latter includes a large contribution from electronic states that do not play a role in bonding. The cohesive energy (E_{coh}) of a given phase is defined as the total energy of the constituent atoms at infinite separation minus the total energy of that particular phase.

The cohesive energy of the compounds in different structures are calculated from the relation

$$E_{coh}^{A_2BC}=[2E_{Atom}^{A}+E_{Atom}^{B}+E_{Atom}^{C}]-E_{Total}^{A_2BC}, \qquad (1)$$

where $E_{Total}^{A_2BC}$ refers to the total energy of the intermetallic compound Ti_2XAl at equilibrium lattice constants and E_{Atom}^{A}, E_{Atom}^{B}, and E_{Atom}^{C} are the atomic energies of the pure constituents.

The formation energy is introduced in order to facilitate a comparison of the stability of phases, as the cohesive and total energies contain large contributions that are irrelevant for the study of phase equilibrium. In order to determine heats of formation, we first calculated the total energies of elemental Ti, V, Zr, Nb, and Al metals corresponding to their respective equilibrium lattice parameters. At zero temperature, there is no entropy contribution to the free energy; therefore, the free energy of formation, or the heat of formation, can be obtained from the following relation:

$$E_{Form}^{A_2BC}=E_{Total}^{A_2BC}-[2E_{Solid}^{A}+E_{Solid}^{B}+E_{Solid}^{C}], \qquad (2)$$

where $E_{Total}^{A_2BC}$ refers to the total energy of Ti_2XAl at equilibrium lattice constants and E_{Solid}^{A}, E_{Solid}^{B}, and E_{Solid}^{C} are the total energy of the pure elemental constituents. The systematic errors in the total energy due to the use of atomic sphere approximation (ASA) are canceled significantly, leading to a reasonably accurate formation energy.

The calculated values of the cohesive energies and heats of formation of all the three systems are given in Tables I, II, and III. The cohesive energy for the three structures does not differ very much, which obiviously indicates the presence of all the three phases in equilibrium at a certain temperature range. The magnitudes of heat of formation in the $B2$ structure have the highest values for of Ti_2NbAl and Ti_2VAl systems and these two systems should be more stable in the $B2$ phase. The heat of formation of Ti_2NbAl in the $D0_{19}$ structure is smaller by 0.031 eV/atom compared to the $B2$ phase and in the O phase, it is still smaller. On the other hand, the heat of formation for Ti_2ZrAl in the three phases (Table III) shows clearly the prefered stability of the $D0_{19}$ phase over the other two phases.

TABLE II. Structural and cohesive properties of the three phases of Ti_2VAl.

Ti_2VAl	$B2$	$D0_{19}$	$O\,(A_2BC)$
Lattice parameters (a.u.)	$a=5.884$	$a=10.482$	$a=10.811$
Calculated		$c=8.579$	$b=17.736$
			$c=8.609$
Cohesive energy E_{coh} (eV/atom)	10.879	10.812	10.696
Heat of formation ΔH (eV/atom)	-0.218	-0.151	-0.021
$N\,(E_F)$ (states/Ry/Cell)	126.84	133.18	149.23
Fermi energy E_F (Ry)	-0.055	-0.035	-0.044
Bulk modulues B (Mbar)	2.129	2.035	2.015
B'	5.596	6.582	5.721

TABLE III. Structural and cohesive properties of the three phases of Ti_2ZrAl.

Ti_2ZrAl	$B2$	$D0_{19}$	$O\,(A_2BC)$
Lattice parameters (a.u.)	$a=6.169$	$a=10.986$	$a=11.298$
Calculated		$c=8.902$	$b=18.935$
			$c=8.997$
Cohesive energy E_{coh} (eV/atom)	10.589	10.640	10.526
Heat of formation ΔH (eV/atom)	−0.153	−0.204	−0.020
$N\,(E_F)$ (states/Ry/cell)	177.25	87.74	162.93
Fermi energy E_F (Ry)	−0.116	−0.106	−0.098
Bulk modulus B (Mbar)	1.572	1.717	1.573
B'	5.167	5.062	4.999

Vinet *et al.*[19] have proposed a universal equation of state for solids which is claimed to be superior to that of the Birch-Murnaghan equation of state[20,21] as it is applicable for all kinds of bonding. According to them, if one defines x as $(V/V_0)^{1/3}$ and $H(x)=x^2P(x)/3(1-x)$, then the $\ln[H(x)]$ verses $(1-x)$ curve should be nearly linear and obey the relation:

$$\ln[H(x)]\simeq \ln B_0+\eta(1-x). \tag{3}$$

The isothermal equation of state (EOS) is expressed as

$$P=[3B_0(1-x)/x^2]\exp[\,\eta(1-x)\,]. \tag{4}$$

The slope of the curve (η) is related to the pressure derivative of the bulk modulus (B_0') by

$$\eta=3/2[B_0'-1]. \tag{5}$$

We calculated the values of $\ln[H(x)]$ and $(1-x)$ using the $P-V$ data and made the least-squares fit in a manner similar to what we have made earlier.[22] From this the bulk moduli and pressure derivative of bulk moduli for the three phases of these alloys were calculated.

The total energies calculated as a function of unit-cell volume for Ti_2NbAl, Ti_2VAl, and Ti_2ZrAl are presented in Figs. 2–4. We have plotted the total energy with respect to a reference energy (E_0) which is indicated in the figures. From these results the equilibrium lattice constants, bulk modulii, and heats of formation are obtained. For Ti_2NbAl in the $B2$ phase (open circle in Fig. 2), the lattice constant and the bulk modulus were determined to be 6.050 a.u. and 1.454 Mbar, respectively. These structural properties obtained from the calculation are given in Table I along with those of the $D0_{19}$ and O phases.

For the $D0_{19}$ phase, we started the calculation with the experimental lattice constants of $a=10.960$ a.u. and $c=8.882$ a.u. with $c/a=0.810$. We then varied the c/a ratio at this volume to get the theoretical c/a ratio. Using this c/a ratio, the total energy was again calculated as a function of unit-cell volume which is shown as open squares in Fig. 2. We obtained the lattice constants a and c as 10.774 and 8.731 a.u., and a bulk modulus of 1.524 Mbar. For the orthorhombic structure, the atomic coordinates are taken from the work of Banerjee *et al.*[6] We varied the experimental a/b and c/b values maintaining the experimental cell volume and by minimizing the energy we obtained $a/b=0.627$ and $c/b=0.485$ through the same total-energy consideration. We then varied the volume with this a/b and c/b values to determine equilibrium volume and lattice constants and these are shown as open diamonds in Fig. 2. From these we obtained the lattice constants as $a=11.337$ a.u., $b=18.057$ a.u., $c=8.765$ a.u., and a bulk modulus of 1.359 Mbar. The theoretical bulk modulus compares well with the experimental bulk modulus of 1.23 Mbar obtained using the relation $B=E/3(1-2\gamma)$, where E is Young's modulus and γ is Poisson's ration.[23] It should be noted that for $D0_{19}$ and $O\,(A_2BC)$ phases, the energy minimization has been achieved with respect to both the axis ratios and unit-cell volumes. The underestimation of the theoretically obtained

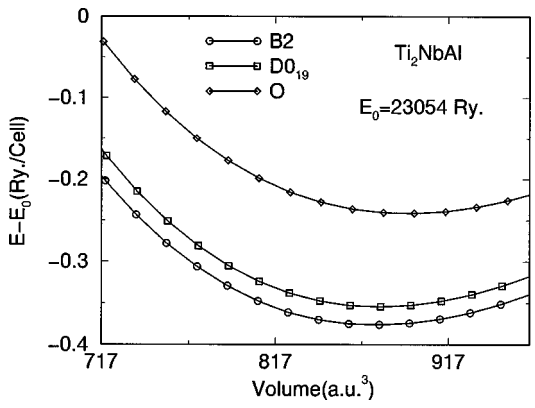

FIG. 2. Total energy vs cell volume in Ti_2NbAl.

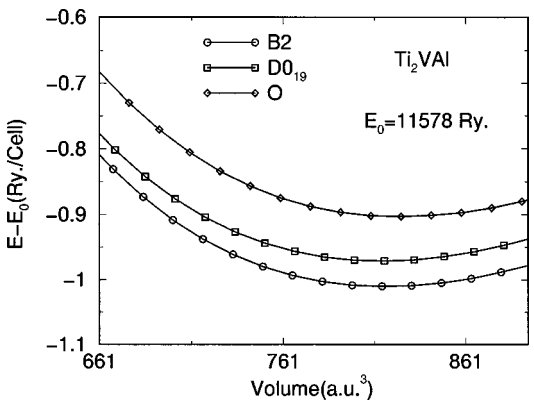

FIG. 3. Total energy vs cell volume in Ti_2VAl.

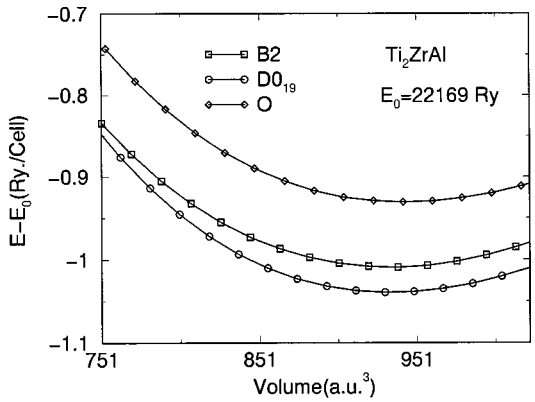

FIG. 4. Total energy vs cell volume in Ti_2ZrAl.

lattice constants by 1–2 % for Ti_2NbAl compared to the experimental value is due to the neglect of zero-point motion and the overestimation of bonding by the LDA, as has been discussed in detail in our earlier work and that of Moruzzi *et al.*[22,24] It can be seen from Fig. 2 that the equilibrium cell volume for the three phases are slightly different being minimum for $B2$ phase. The relatively large bulk modulus and smaller lattice parameter of the $B2$ phase can be attributed to its better fracture toughness. In comparison to the lattice parameters of the $D0_{19}$ phase of Ti_3Al, most of the parameters are increased by 1–3 %. This can be attributed to the high content of large Nb atoms in Ti_2NbAl alloy phases.

The calculated structural and cohesive properties of Ti_2VAl and Ti_2ZrAl are given in Tables II and III, respectively. The total-energy calculations shows that Ti_2VAl and Ti_2NbAl systems crystallize in the $B2$ phase (Figs. 2 and 3) whereas the Ti_2ZrAl system has $D0_{19}$ structure as its ground state (Fig. 4). These observarions are in agreement with the heats of formation reported in the tables as one would normally expect. The calculated lattice parameters of Ti_2NbAl agree well with the experimental values. As Nb and V atoms belong to the same group, the insertion of V atoms at the Nb site shows the obvious compression of the lattice and accordingly we observe that the lattice parameters corresponding to Ti_2VAl are smaller than that of Ti_2NbAl systems as expected. The dilation of the lattice due to the replacement of Nb with Zr is also observed which may be seen in Table III.

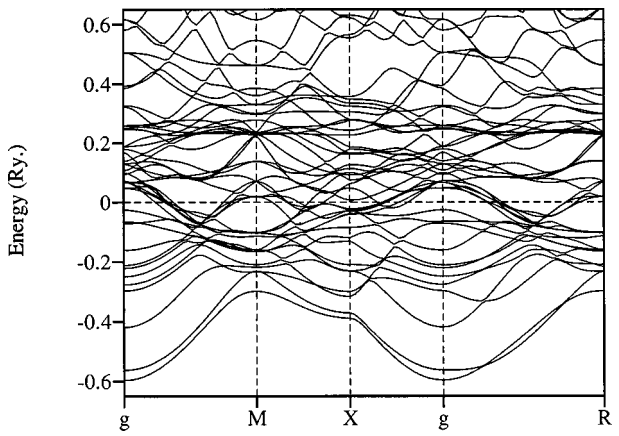

FIG. 5. Calculated band structure of Ti_2NbAl in stable $B2$ phase. The Fermi energy is denoted by the horizontal line at $E=0$ in all the three band-structure plots.

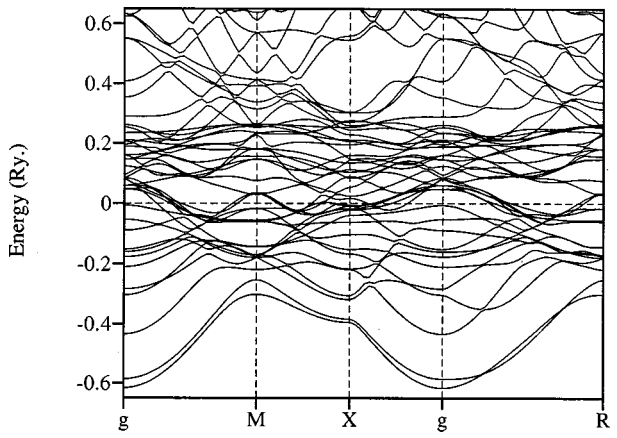

FIG. 6. Calculated band structure of Ti_2VAl in the stable $B2$ phase.

IV. BAND STRUCTURE, DENSITY OF STATES, AND BONDING

The calculated energy bands corresponding to the stable phases of Ti_2XAl are shown in Figs. 5–7. It may be seen (Figs. 5–7) that the low-lying two bands, which give rise to the low-energy tail in the DOS, are nearly parabolic, and it is mainly due to the Al s states. The higher-lying bands in the vicinity of Fermi energy are primarily Ti-d and X-d derived states, although as is evident from the DOS there is significant hybridization of these states with the Al-p orbitals. In order to see the influence of crystal structures on the density-of-states distribution, we have presented the DOS for all the three structures ($B2$,$D0_{19}$,O) of these systems in Figs. 8–10. From the plots of the density of states we can see that the low-lying two bands are mainly due to the Al-s orbitals as stated earlier. They are separated from the higher-lying p-d bands by a small gap for the $D0_{19}$ phase whereas in the case of $B2$ and O phases the separation is not seen as it displays a weak hybridization with the higher bands. This feature is exhibited by all the three systems and this shows

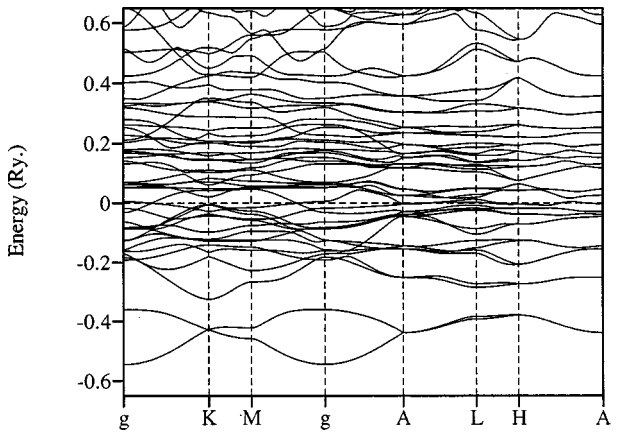

FIG. 7. Calculated band structure of Ti_2ZrAl in the stable $D0_{19}$ phase.

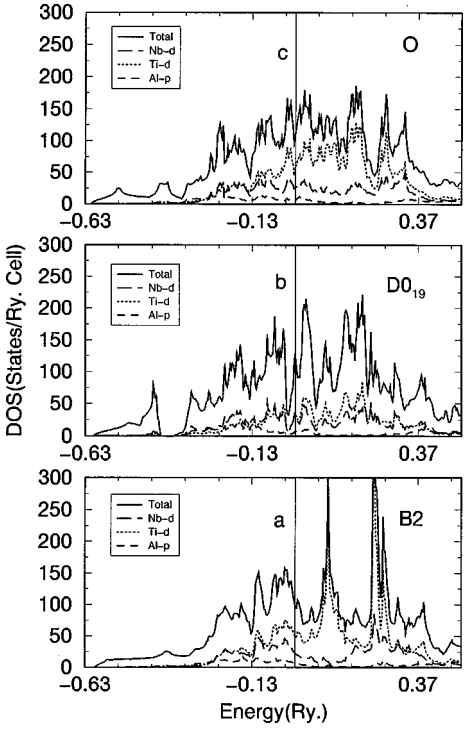

FIG. 8. Density of states of Ti_2NbAl in $B2$, $D0_{19}$, and O phases.

that it is inessential whether the Al-*s* bands hybridize with other bands or not in respect of the structural stability. We can also see, in the DOS plots of Ti_2NbAl and Ti_2VAl, that in $B2$ structure not all the bonding states are filled, in $D0_{19}$ structure antibonding states are partially occupied, and in O structure the bonding and antibonding separation is not so pronounced, and that in all the three structures most of the

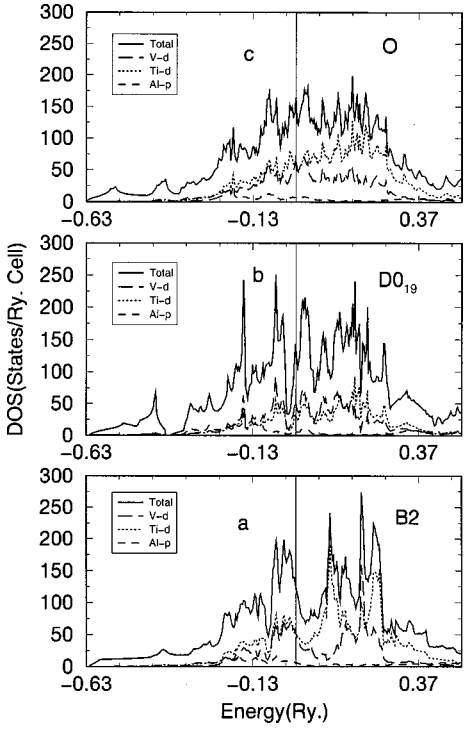

FIG. 9. Density of states of Ti_2VAl in $B2$, $D0_{19}$, and O phases.

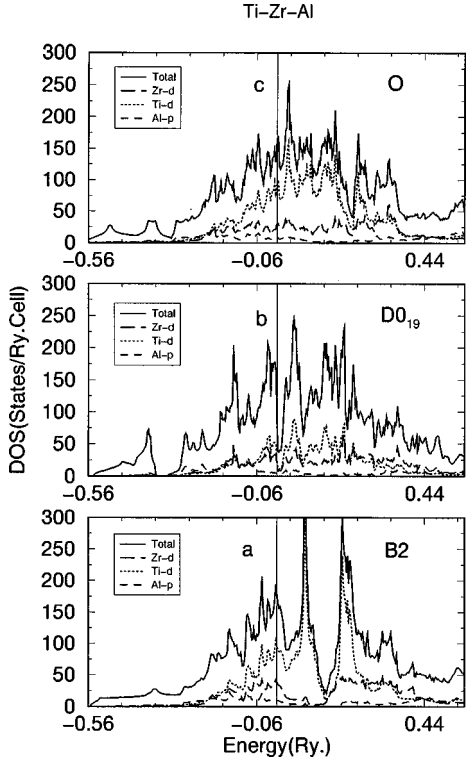

FIG. 10. Density of states of Ti_2ZrAl in $B2$, $D0_{19}$, and O phases.

atom-projected DOS overlap over large energy range. It can be seen that the *d-d* hybridization and *p-d* hybridization among Ti (Nb,V) and Al appears in all the three phases; however, these interactions exhibit different features for the three phases. For the cubic $B2$ and hexagonal $D0_{19}$ structure, the DOS exibits a prominent feature, a well separated bonding and antibonding region and these two regions are separated by a deep valley. In the $D0_{19}$ structure, the Fermi level is located in the antibonding region. The $B2$ structure, in which the Fermi level is located in the bonding region of DOS, is more stable compared to $D0_{19}$ and orthorhombic structures.[25] The pseudogap feature has disappeared in the orthorhombic structure with a hallow in the DOS at Fermi energy which is shallow. This might be due to the relatively weak *d-d* and *p-d* interplanar interactions possible in this structure as compared to the other two phases. The correlation of the Fermi level falling at the pseudogap to structural stability is not always obeyed if the materials have metastability or martensitic transformation.[26,27]

The density of states at Fermi energy $[N(E_F)]$ are listed in Tables II and III for the $B2$, $D0_{19}$, and O phases. The lowest value of $N(E_F)$ shows the higher stability of the $B2$ phase in these two compounds compared to the other two phases.[28] However, the values of $N(E_F)$ do not differ very much in the three phases, indicating the possibility of the three phases to be in equilibrium over a temperature range. Thus, the calculated results are in favor of the experimental observation that within a narrow temperature range, between 950 °C and 1000 °C, all the three phases might be in equilibrium.[7] Recent results on equilibrium phases in orthorhombic alloys with a constant 22 at. % Al indicates the existence of such a three-phase field.[29]

It can be seen from the DOS plots of Ti_2ZrAl (Fig. 10)

TABLE IV. Atomic distance (a.u.) and the coordination in Ti_2NbAl. Only neighbors of appreciable overlap are shown. NN stands for nearest neighbor.

	$B2$		$D0_{19}$		$O(A_2BC)$	
Ref. atom	Distance	NN	Distance	NN	Distance	NN
Ti	5.239 59	4Nb+4Al	5.360 08	2Al+2Nb+2Ti	5.315 99	2Ti
			5.387 31	2Nb+2Ti+2Al	5.330 32	2Al+2Nb
					5.432 42	2Al+2Nb
Nb	5.239 59	8Ti	5.360 28	2Al+2Nb+2Ti	5.315 99	2Nb
	6.050 16	4Nb+2Al	5.387 10	4Ti+2Al	5.330 32	4Ti
					5.432 42	4Ti
Al	5.239 59	8Ti	5.360 28	4Ti+2Nb	5.318 04	2Al
	6.050 16	4Al+2Nb	5.387 31	4Ti+2Nb	5.331 85	4Ti
					5.431 92	4Ti

that both in $B2$ and $D0_{19}$ structures, the Fermi level lies in the bonding region. However, the $[N(E_F)]$ in the $D0_{19}$ phase is low compared to the $B2$ phase and the pseudogap is very prominent in the $D0_{19}$ phase. Further, the Fermi level falls very close to the pseudogap in the $D0_{19}$ phase and this feature strongly favors the ordering of this alloy in $D0_{19}$ phase.

The interatomic distances and the coordination numbers for the Ti_2NbAl system are given in Table IV. This alloy that has been found to stabilize in the $B2$ phase satisfies the so-called space filling principle and the symmetry principle with respect to the stability of the intermetallic systems. In the $B2$ phase, the nearest-neighbor distance has the shortest value of 5.239 a.u. and the highest coordination number of 8. Further among the structures considered it has the highest symmetry. The shortest interatomic distances imply strong bonding. In the case of Ti_3Al, TiAl, $TiAl_3$, the covalent $pd\sigma$ bonding is primarily due to the Ti-3d interaction with Al-2p electrons. Whereas in the case of Ti_2NbAl, the d-d bonding between Ti and Nb enhances metallicity in the system at the expense of $pd\sigma$ bonding, leading to greater ductility and fracture toughness. However, it should be emphasized that according to Villars[30] the stability of the crystal structures of the intermetallics depend on several other factors. As far as Ti_2ZrAl is concerned, the other factors seem to dominate and make it stable in the $D0_{19}$ phase. For the sake of comparison, the ground-state properties of Ti_3Al, TiAl, $TiAl_3$ collected from the literature are given in Table V along with the calculated values of Ti_2XAl alloys.

V. SUMMARY AND CONCLUSION

The structural stability and cohesive properties of Ti_2XAl (X=Nb, V, Zr) in $B2$, $D0_{19}$, and O phases have been studied theoretically, using the results of the electronic structure and total-energy calculations. The results were further used to evaluate the equilibrium lattice parameters, cohesive energy, heat of formation, and bulk modulii of these alloys. The total-energy curves corresponding to the $B2$, $D0_{19}$, and O phases of these alloys are close in energy and it demonstrates the possibility of the presence of all the three phases at some particular range of thermodynamic conditions. Our calculations predict the $B2$ phase as the stable phase of Ti_2NbAl and Ti_2VAl at equilibrium conditions, whereas the $D0_{19}$ phase is found to be stable for the Ti_2ZrAl. Further, Fig. 10 shows a possible structural transition from the $D0_{19}$ to $B2$ phase under strong compression in Ti_2ZrAl. The theoretically calculated equilibrium lattice parameters of Ti_2NbAl are found to be in good agreement with the experimental values whereas the experimental lattice parameters of Ti_2VAl and Ti_2ZrAl are not available and hence we could not make a comparison.

The density-of-states histogram of these three systems exhibit similar features in the respective structures. The concept of pseudogaps, i.e., the sharp drop in the density of states at or in the vicinity of the Fermi level that has been prominently displayed by the binary Ti-Al systems arising out of the strong Ti(3d) and Al(2p) mixing and the stability considerations as well as other correlations that have been

TABLE V. Cohesive properties of Ti-Al based alloys.

Properties	Ti_3Al[a]	TiAl[b]	$TiAl_3$[c]	Ti_2NbAl	Ti_2VAl	Ti_2ZrAl
R_{ws} (a.u.)	2.98	2.91	2.92	2.97	2.89	3.12
$N(E_F)$ (states/Ry/f.u.)	26.52	23.54	24.40	47.58	63.42	43.87
Heat of formation (eV/atom)	0.25	0.46	0.42	0.24	0.22	0.20
Bulk modulus (Mbar)	1.3	1.28	1.20	1.45	2.13	1.72

[a]Reference 31.
[b]Reference 32.
[c]Reference 28.

discussed at length,[28] is not strongly demonstrated in these ternary systems. Even though the pseudogap is present, the values of $N(E_F)$ are not as small as those obtained in binary systems and this is due to the enhanced d-d interaction arising out of the Ti($3d$) and $X(3d/4d)$ electrons that enhance metallicity at the expense of $pd\sigma$ bonding present in the binary systems. The better ductility realized in multiphase Ti_2NbAl can be attributed to the relatively elevated $N(E_F)$ in all its three phases. Our calculation shows an increase in the cohesive energy in Ti_2NbAl compared to Ti_3Al and it reveals the increase in the bond strength. In conclusion, the present work yields useful information on the trends of the structural stability and cohesive properties of the Ti-Al-based ternary systems, and this work will form the basis for future study on quaternary systems.

ACKNOWLEDGMENTS

C.R. gratefully acknowledges financial support from DST, India, and Dr. D. Banerjee, and his group at DMRL, for support at different stages of the work.

[1] R. von Mises, Z. Angew. Math. Mech. **8**, 161 (1928).
[2] D. G. Konitzer, I. P. Jones, and H. L. Fraser, Scr. Metall. **20**, 265 (1986).
[3] T. K. Nandy, D. Banerjee, and A. K. Gogia, in *Proceedings of the 6th World Conference on Titanium*, edited by P. Lacombe, R. Tricot, and G. Beranger (Les Ulis, France, 1988), Vol. II, pp. 943–948.
[4] D. Banerjee, T. K. Nandy, and A. K. Gogia, Scr. Metall. **21**, 597 (1987).
[5] D. Banerjee, A. K. Gogia, T. K. Nandy, and V. A. Joshi, Acta Metall. **36**, 871 (1988).
[6] D. Banerjee, T. K. Nandy, and A. K. Gogia (unpublished).
[7] J. Kumpfert and C. Leyens, *Structural Intermetallics 1997*, edited by M. V. Nathal, R. Darolia, C. T. Liu, P. L. Martin, B. Miracle, R. Wagner, and M. Yamaguchi (The Minerals Metals and Materials Society, Warrendale, Pennsylvania,, 1997), pp. 895–904.
[8] M. J. Blackburn and M. P. Smith, US Air Force Technical Report No. AFML-TR-78-18, Wright Patterson Air Force Base, Dayton, OH (1978).
[9] D. Banerjee, in *Intermetallic Compounds—Principles and Practice*, edited by J. H. Westbrook and R. L. Fleischer (Wiley, New York, 1995), Vol. 2, Chap. 5, pp. 101–131.
[10] A. K. Gogia, T. K. Nandy, D. Banerjee, T. Carisey, J. L. Studel, and J. M. Franchet, Intermetallics **6**, 741 (1998).
[11] M. van Schilfgaarde, A. T. Paxton, A. Pasturel, and M. Methfessel, *Alloy Phase Stability and Design*, edited by G. M. Stocks *et al.*, Materials Research Society Symposia No. 186 (Materials Research Society, Pittsburgh, 1990), p. 107.
[12] D. G. Pettifor, Mater. Sci. Technol. **8**, 345 (1992).
[13] M. Sluiter, D. de Fontaine, X.-Q. Guo, R. Podloucky, and A. J. Freeman, Phys. Rev. B **42**, 10 460 (1990).
[14] M. Asta, D. de Fontaine, M. van Schilfgaarde, M. Sluiter, and M. Methfessel, Phys. Rev. B **46**, 5055 (1992).
[15] O. K. Andersen, Phys. Rev. B **12**, 3060 (1975).
[16] H. L. Sriver, *The LMTO Method* (Springer, Heidelberg, 1984).
[17] O. K. Andersen and O. Jepsen, Phys. Rev. Lett. **53**, 2571 (1984).
[18] O. K. Anderson, in *Methods of Electronic Structure Calculations*, edited by O. K. Andersen, V. Kumar, and A. Mookerjee (World Scientific, Singapore, 1994).
[19] P. Vinnet, J. Ferrante, J. R. Smith, and J. H. Rose, J. Phys. C **19**, L467 (1986).
[20] F. D. Murnaghan, Proc. Natl. Acad. Sci. USA **30**, 244 (1944).
[21] F. Birch, J. Geophys. Res. **83**, 1257 (1978).
[22] P. Ravindran and R. Asokamani, Phys. Rev. B **53**, 1129 (1996).
[23] T. K. Nandy and D. Banerjee, *Structural Intermetallics 1997*, edited by M. V. Nathal, R. Wagner, and M. Yamaguchi (The Minerals Metals and Materials Society, Warrendale, Pennsylvania, 1997), p. 777.
[24] V. L. Moruzzi, J. F. Janak, and K. Schwarz, Phys. Rev. B **37**, 790 (1988).
[25] J. H. Xu and A. J. Freeman, Phys. Rev. B **41**, 12 553 (1990).
[26] P. Ravindran and R. Asokamani, Phys. Rev. B **50**, 668 (1994).
[27] R. Kuentzler and R. W. Waterstrat, J. Less-Common Met. **125**, 261 (1986).
[28] T. Hong, T. J. Watson-Yong, A. J. Freeman, T. Oguchi, and J.-h. Xu, Phys. Rev. B **41**, 12 462 (1990).
[29] D. B. Miracle, M. A. Foster, and C. G. Rhodes, *Phase Equilibria in Ti-Al-Nb Orthorhombic Alloys*, Titanium'95, edited by P. A. Blenkinsop, W. A. Evans, and H. M. Flower (The Institute of Materials, London, 1995), pp. 372–378.
[30] P. Villars, in *Intermetallic Compounds—Principles and Practice*, Ref. 9, Vol. 1, Chap. 11, pp. 227–275.
[31] T. Hong, T. J. Watson-Yang, X.-Q. Guo, A. J. Freeman, T. Oguchi, and Jian-hua Xu, Phys. Rev. B **43**, 1940 (1991).
[32] W. Wolf, R. Podloucky, P. Rogl, and H. Erschbaumer, Intermetallics **4**, 210 (1996).